ORIGINAL PAPER

Spatial representativeness of single tower measurements and the imbalance problem with eddy-covariance fluxes: results of a large-eddy simulation study

**Gerald Steinfeld · Marcus Oliver Letzel ·
Siegfried Raasch · Manabu Kanda · Atsushi Inagaki**

Abstract   A large-eddy simulation (LES) study is presented that investigates the spatial variability of temporal eddy covariance fluxes and the systematic underestimation of representative fluxes linked to them. It extends a prior numerical study by performing high resolution simulations that allow for virtual measurements down to 20 m in a convective boundary layer, so that conditions for small tower measurement sites can be analysed. It accounts for different convective regimes as the wind speed and the near-surface heat flux are varied. Moreover, it is the first LES imbalance study that extends to the stable boundary layer. It reveals shortcomings of single site measurements and the necessity of using horizontally-distributed observation networks. The imbalances in the convective case are attributed to a locally non-vanishing mean vertical advection due to turbulent organised structures (TOS). The strength of the TOS and thus the imbalance magnitude depends on height, the horizontal mean wind and the convection type. Contrary to the results of a prior study, TOS cannot generally be responsible for large energy imbalances: at low observation heights (corresponding to small towers and near-surface energy balance stations) the TOS related imbalances are generally about one order of magnitude smaller than those in field experiments. However, TOS may cause large imbalances at large towers not only in the case of cellular convection and low wind speeds, as found in the previous study, but also in the case of roll convection at large wind speeds.

In the stably stratified boundary layer for all observation heights neither TOS nor significant imbalances are observed.

G. Steinfeld (✉) · M. O. Letzel · S. Raasch
Institut für Meteorologie und Klimatologie, Universität Hannover,
Hannover, Germany
e-mail: steinfeld@muk.uni-hannover.de

M. Kanda · A. Inagaki
Department of International Development Engineering,
Tokyo Institute of Technology,
Tokyo, Japan

Attempting to reduce imbalances in convective situations by applying the conventional linear detrending method increases the systematic flux underestimation. Thus, a new filter method is proposed.

1 Introduction

All physical processes that take place on scales smaller than the grid spacing of an atmospheric simulation model must be parameterised. Thus, the interaction between the atmosphere, vegetation and the underlying surface is included in most atmospheric models by corresponding parameterisation schemes. Generally, the development and validation of such schemes can only be as accurate as the measurements they are based on.

The most widespread technique for the measurement of vertical fluxes (e.g. the sensible heat flux) is the eddy-covariance (EC) method. By application of the so-called spatial EC method turbulent fluxes are determined by an evaluation of the horizontal average of the spatial covariances of the vertical velocity and the transported scalar. Schröter et al. (2000) pointed out that this method does not cause any bias in the evaluation of the representative heat flux for a horizontally homogeneous domain. However, a prerequisite for its successful application is the availability of spatially dense, simultaneous measurements of the transported quantity and the vertical velocity throughout the domain under consideration. Unfortunately, this prerequisite cannot be met by currently available measurement systems.

For most field campaigns time series from ground-based measurements at only a few sites within the investigated domain are available, and are used to evaluate fluxes by applying the so-called temporal EC method, in which the temporal average of the covariances of the transporting and the transported quantity with regard to time is determined. Mahrt (1998) reports on a discrepancy between turbulent fluxes obtained from aircraft-based measurements (spatial EC method) and those calculated from local time series (temporal EC method). His finding is supported by observations from further field campaigns reviewed in Isaac et al. (2004). Katul et al. (1999), analysing measurements at seven towers over a horizontally homogeneous pine forest, found a standard deviation of about 17% for the turbulent sensible heat flux and 33% for the latent heat flux. Furthermore, it is a widespread observation in field experiments (e.g. Twine et al. 2000; Panin et al. 1998; Beyrich et al. 2002) that the sum of sensible and latent heat flux underestimates the sum of the net radiation and ground heat flux, i.e. the fundamental law of energy conservation is appearently violated. This highlights the need to check the suitability of the temporal EC method for the determination of spatially representative fluxes, which is imperative for the accurate modelling of surface energy and mass balances. According to Foken (2003) underestimates of heat fluxes by 10–30% are observed in field campaigns. He points out that imbalances can also be observed in the stably stratified, nocturnal atmospheric boundary layer, and Wilson et al. (2002) report that at FLUXNET sites the largest imbalances are observed at night.

In this context, the investigation of the energy imbalance problem is gaining increasing importance, but even the EBEX-2000 field experiment, designed to study the lack

of an energy balance, could not identify its sources (Oncley et al. 2002). Nevertheless, several causes for the energy imbalance have been discussed to date, e.g. see Mahrt (1998) and Twine et al. (2000). These can partly be attributed to errors and uncertainties in the measurement set-up (e.g. sensor errors or a mismatch between the footprints of different energy fluxes). Other potential causes are related to flow structures in the atmospheric boundary layer.

In the present study, we simulated multi-point measurements of turbulent quantities by using the large-eddy simulation (LES) model PALM. Therefore, errors due to uncertainties in field conditions or sensor shortcomings are avoided, and this allows us to investigate the causes of imbalances and the spatial variability of temporal EC fluxes related to flow properties. The concept of a numerical investigation of the imbalance problem used here has been presented by Kanda et al. (2004) (Ka04). Ka04 found that the EC flux based on a point measurement systematically underestimates the representative flux, and attributed the resulting negative imbalance to the existence of turbulent organised structures (TOS); they related the large scatter of flux estimates to the temporal and spatial change of TOS patterns. Moreover, they pointed out a clear dependency of the imbalance statistics on the geostrophic wind, and found some evidence for a dependency of imbalances on height. Our study ties in with the questions arising from their paper. Ka04 restricted their investigation to the convective boundary layer (CBL) and to observation heights above 50 m. The limited resources of supercomputers made it impossible for Ka04 to carry out virtual measurements at heights common to small tower EC sites or even near-surface energy balance stations. Moreover, the limitations prevented an extension of their study to the stable boundary layer (SBL), where LES requires an even higher spatial resolution (Beare et al. 2006). Increasing computer power now enables us for the first time to investigate whether Ka04's mechanism is also of relevance at the measurement heights of small tower EC sites and whether there is a similar mechanism in the SBL. Also, we attempt to clarify the impact of strong horizontal wind and near-surface heat flux magnitude on the energy imbalance.

The article is organised as follows. Sect. 2 provides the theoretical background, and Sect. 3 provides relevant details on the applied LES model and the simulations. The results are described and discussed in Sect. 4. In Sect. 5 we assess the impact of both conventional and proposed new filter methods on the magnitude of imbalances. Finally, we summarise our results and point out some conclusions for the design of field experiments.

2 Theoretical background

The representative kinematic heat flux is defined here as the spatial and temporal mean of the local instantaneous vertical kinematic heat flux F

$$F = w(\Theta - \Theta_b) = w\Theta - w\Theta_b, \tag{1}$$

where w is the vertical velocity (m s^{-1}), Θ (K) is the potential temperature and Θ_b (K) is a reference temperature. Θ_b has to be considered because the heat carried by an air parcel due to an input of heat at the ground surface is related to its temperature change and not to its absolute temperature (e.g. Webb et al. 1980; Leuning and Legg 1982).

If $[\varphi]$ denotes the horizontal average of a quantity φ over a certain horizontal domain and if $\overline{\varphi}$ denotes the temporal average of a quantity φ over a certain period of time, then the representative flux $[\overline{F}]$ can be written as

$$\left[\overline{F}\right] = \left[\overline{w\Theta}\right] - \left[\overline{w\Theta_b}\right]. \tag{2}$$

If w and Θ are split up into a horizontal mean and a related deviation (marked by a prime and subscript s), i.e.

$$w = [w] + w'_s, \tag{3}$$
$$\Theta = [\Theta] + \Theta'_s, \tag{4}$$

the representative flux can be evaluated as follows

$$\left[\overline{F}\right] = \overline{[F]} = \overline{[w][\Theta]} + \overline{[w'_s\Theta'_s]} - \overline{[w\Theta_b]}. \tag{5}$$

Under horizontally homogeneous conditions the reference temperature Θ_b might be constant at any height (Webb et al. 1980; Mahrt 1998). Thus, the representative kinematic heat flux can be expressed as

$$\left[\overline{F}\right] = \overline{[w][\Theta - \Theta_b]} + \overline{[w'_s\Theta'_s]}. \tag{6}$$

As Webb et al. (1980) have pointed out there is usually a non-zero mean vertical wind speed $[w]$ due to the correlated fluctuations of the vertical velocity and air density, whenever there is a turbulent flux of heat. Thus, generally the first term on the right-hand side of Eq. 6 does not vanish. However, e.g. Bernhardt and Piazena (1988) reported that the magnitude of the mean vertical velocity $[w]$ amounts only to 10^{-4}–10^{-3} m s^{-1}. Following Webb et al. (1980) the mean vertical velocity $[w]$ could be estimated by the following Eq.

$$[w] = \left[w'_s\Theta'_s\right] / [\Theta]. \tag{7}$$

Taking into account that the temperature difference $[\Theta - \Theta_b]$ is mostly only a small fraction of the mean temperature $[\Theta]$ we can state that the contribution of the first term on the right-hand side of Eq. 6 to the total flux is negligible in any case, so that the representative flux can be determined very accurately as

$$\left[\overline{F}\right] = \overline{[w'_s\Theta'_s]}. \tag{8}$$

Many numerical models including PALM make use of the Boussinesq approximation with a constant mean density, which describes turbulent motions accurately in the case of shallow convection. The application of the Boussinesq approximation effectively filters out sound waves and thus reduces the computing time considerably. However, its application leads to a vanishing horizontally-averaged vertical velocity in the case of cyclic boundary conditions and $w = 0$ at the bottom boundary of the model domain, which is contrary to the existence of a mean vertical velocity in the real convective boundary layer according to Webb et al. (1980). However, according to the remarks that led us from Eq. 6 to Eq. 8 the impact of the non-vanishing mean vertical velocity on the flux evaluation is negligible, so that a comparison between field fluxes and simulated fluxes is justified.

The representative flux can hence be obtained without any significant systematic error by evaluating temporal averages of so-called spatial EC fluxes.

In most field experiments only ground-based measurements at a few sites are available. In these cases w and ϕ are decomposed into a temporal mean and a deviation (marked by a prime and subscript t), i.e.

$$w = \overline{w} + w_t', \tag{9}$$

$$\Theta = \overline{\Theta} + \Theta_t'. \tag{10}$$

Assuming the ideal (unrealistic) case of a horizontally dense network of EC sites, and applying the rules of Reynolds averaging on the data, the representative flux can be determined as

$$\left[\overline{F} \right] = \left[\overline{w\Theta} \right] + \left[\overline{w_t'\Theta_t'} \right] - \left[\overline{w\Theta_b} \right]. \tag{11}$$

Further, assuming that the reference temperature is constant under horizontally homogeneous conditions, Eq. 11 can be transformed into

$$\left[\overline{F} \right] = \left[\overline{w \left(\Theta - \Theta_b \right)} \right] + \left[\overline{w_t'\Theta_t'} \right]. \tag{12}$$

Splitting up the actual vertical velocity w into the mean vertical velocity $[w]$ and the corresponding deviation w_s' transforms Eq. 11 into

$$\left[\overline{F} \right] = \left[\overline{[w] \left(\Theta - \Theta_b \right)} \right] + \left[\overline{w_s' \left(\Theta - \Theta_b \right)} \right] + \left[\overline{w_t'\Theta_t'} \right]. \tag{13}$$

For the same reasons as presented in the discussion of Eq. 6, Eq. 13 can be transformed to

$$\left[\overline{F} \right] = \left[\overline{w\Theta} \right] + \left[\overline{w_t'\Theta_t'} \right], \tag{14}$$

since in that case $w_s' = w$ and the condition of horizontal homogeneity applies for the reference temperature Θ_b. In field experiments the first term on the right-hand side of Eq. 13 is neglected, because the total flux is closely represented by the uncorrected covariance alone (see e.g. Webb et al. 1980; Leuning and Legg 1982). Note that these studies deny the existence of the second term of Eq. 13, which is at least questionable.

The second term on the right-hand side of Eq. 14 is the horizontal mean of the so-called temporal EC flux that is determined in tower observations. Equation 14 reveals that even in the case when a spatially dense network of observations is available, the temporal EC method is inappropriate for evaluating the representative flux, as long as the horizontal mean of the local vertical advection term $[\overline{F}]$ does not vanish.

If ground-based measurements of fluxes take place at single sites, the single site temporal EC flux is applied to estimate the representative flux. The deviation of a single temporal EC flux from the representative flux is a measure for the magnitude of the local imbalance I. This measure can be specified relative to the representative flux by

$$I = \left(\overline{w_t'\Theta_t'} - \left[\overline{F} \right] \right) \Big/ \left[\overline{F} \right]. \tag{15}$$

The standard deviation of the local imbalance is an appropriate measure for studying the magnitude of the spatial variability of the temporal EC fluxes. Moreover, the horizontal mean of I,

$$[I] = \left(\left[\overline{w_t'\Theta_t'} \right] - \left[\overline{F} \right] \right) \Big/ \left[\overline{F} \right] = \left[\overline{w\Theta_b - \Theta} \right] \Big/ \left[\overline{F} \right] = - \left[\overline{w\Theta} \right] \Big/ \left[\overline{F} \right], \tag{16}$$

is an appropriate measure for quantifying the systematic error that is related to the temporal EC method. Note that the third form of Eq. 16 is only valid under the

assumption of a vanishing mean value of the vertical velocity, as is the case in our simulations. Equation 16, which is similar to Eq. 3 in Mahrt (1998), reveals that the existence of flow structures causing a non-vanishing horizontal mean of the local vertical advection (e.g. turbulent structures with a time scale that exceeds the averaging period) leads to a flux underestimation. Notice that in the case of a Boussinesq fluid, as in our simulations, Eqs. 15 and 16 are also directly applicable for the evaluation of imbalance statistics of the sensible heat flux.

3 LES model and set-up of simulations

3.1 The LES model

The parallelised large-eddy simulation model PALM (Raasch and Etling 1998; Raasch and Schröter 2001) has been used to simulate multi-point measurements of the vertical velocity w and the potential temperature Θ. A detailed documentation of PALM is available online (Raasch 2006). To date, PALM has been applied to the investigation of the homogeneous (Schröter et al. 2000) and heterogeneous heated CBL (e.g. Raasch and Harbusch 2001; Letzel and Raasch 2003) as well as of the stably stratified boundary layer (Beare et al. 2006). PALM solves both the Navier–Stokes equations in Boussinesq form and an equation for the first law of thermodynamics. As PALM uses a 1.5-order subgrid closure scheme based on Deardorff (1980), it also solves a prognostic equation for the turbulent kinetic energy (TKE). The constraint of a vanishing divergence of the simulated flow at any time and at any grid point of the model domain is met by solving a Poisson equation for the perturbation pressure with the means of fast Fourier transformation (FFT). The lateral boundaries are cyclic and the validity of Monin-Obukhov similarity theory is assumed between the surface and the first computational grid point of the model domain. Second-order finite differences are used to discretise the differential equations and for the temporal integration a leapfrog scheme is applied. The horizontally-averaged mean vertical wind velocity is zero due to the application of the Boussinesq equation with a constant density, in combination with a vanishing vertical velocity at the ground and at the top as boundary conditions.

An overview of the parameters used in the performed simulations is presented in Table 1.

3.2 Set-up of high resolution simulations

Simulations with a set-up similar to that described in detail in Ka04 were carried out, but the grid spacing was drastically reduced from 50 to 10 m. This allowed us to study the imbalance problem for the CBL upwards from a height of 20 m (where the subgrid-scale contribution to the total flux is already smaller than 6%), and therefore for the first time within the range of observation heights at small tower EC sites (e.g. Bosveld and Bouten 2001; Bosveld and Beljaars 2001). The initialisation of the vertical profile of the potential temperature, with a gradient of $0.8 \, \mathrm{K \, km^{-1}}$ up to 1200 m and $7.4 \, \mathrm{K \, km^{-1}}$ above, the horizontally homogeneous near-surface heat flux ($0.1 \, \mathrm{K \, m \, s^{-1}}$), and the roughness length (0.1 m) were chosen as in Ka04. Due to the increased spatial resolution the constant timestep had to be reduced to 0.08 s (Ka04 used 0.4 s). Two high resolution runs have been carried out (C1 and C2) using different values of the geostrophic wind.

Table 1 Survey on the parameters of the performed simulations of the convective (Ci) and the stable (S1) boundary layer. Δ: grid spacing; u_{g}: geostrophic wind; F_{Θ}: near-surface heat flux; dt: timestep; t_{s}: total simulation time

Run	Gridpoints	Δ(m)	$u_{\mathrm{g}}(\mathrm{m\,s^{-1}})$	$F_{\Theta}(\mathrm{K\,m\,s^{-1}})$	dt(s)	t_s(h)
C1	$840 \times 840 \times 240$	10	0	0.1	0.08	5
C2	$840 \times 840 \times 240$	10	2	0.1	0.08	5
C3	$240 \times 240 \times 64$	50	0	0.05	0.4	5
C4	$240 \times 240 \times 64$	50	0	0.1	0.4	5
C5	$240 \times 240 \times 64$	50	0	0.2	0.4	5
C6	$240 \times 240 \times 64$	50	0	0.3	0.4	5
C7	$240 \times 240 \times 64$	50	0	0.4	0.4	5
C8	$240 \times 240 \times 64$	50	2	0.05	0.4	5
C9	$240 \times 240 \times 64$	50	2	0.1	0.4	5
C10	$240 \times 240 \times 64$	50	2	0.2	0.4	5
C11	$240 \times 240 \times 64$	50	2	0.3	0.4	5
C12	$240 \times 240 \times 64$	50	2	0.4	0.4	5
C13	$240 \times 240 \times 64$	50	15	0.05	0.4	5
S1	$192 \times 192 \times 192$	2	8	-0.0075	0.1	11

3.3 Set-up of simulations for sensitivity studies

We continued Ka04's parameter studies on imbalance statistics by investigating the dependency of imbalances on the near-surface heat flux magnitude and on geostrophic wind velocities (simulations C3–C13). All initial and boundary conditions were chosen as in simulation E1 of Ka04.

3.4 Set-up for the simulation of the stable boundary layer

We used the parameters of Beare et al. (2006) for the SBL simulation (run S1). However, in order to allow for the simulation of a boundary layer in a quasi-stationary state, and in order to prevent inhomogeneous near-surface fluxes, we prescribed a homogeneous near-surface kinematic heat flux of $-0.0075\,\mathrm{K\,m\,s^{-1}}$ that gave similar boundary-layer development as that described in Beare et al. (2006) where the surface temperature had been prescribed. Furthermore, the temperature profile was initialised with a constant value of 265 K up to 100 m and a gradient of $10\,\mathrm{K\,km^{-1}}$ above. In order to trigger turbulence a random perturbation of amplitude 0.1 K and zero mean was added to the temperature field below a height of 50 m at the onset of the simulation (Beare et al. 2006). After 9 h of simulated time (using a timestep of 0.1 s) the turbulent flow had reached a quasi-equilibrium state satisfying the mean wind criteria described in Beare et al. (2006).

4 Results

4.1 Near-surface imbalance and spatial variability of turbulent fluxes

Ka04 have already studied the dependence of the imbalance statistics on the observation height. Analysing virtual measurements at four heights between 50 and 125 m, they found that the spatial variability of temporal EC fluxes, as well as the horizontal

Table 2 Imbalance statistics for runs with high spatial resolution. z_a: height analysed; u_g: geostrophic wind; t_p: time period elapsed from simulation start; $[I]$: horizontal average of local imbalances; σ_I: standard deviation of local imbalances; SGS: subgrid-scale contribution to the total flux

Run	z_a (m)	u_g (m s^{-1})	t_p (h)	$[I]$ (%)	σ_I (%)	SGS (%)
C1	20	0	2–3	5.69	17.61	5.15
	30	0	2–3	7.81	22.48	4.23
	50	0	2–3	11.47	30.60	1.82
	80	0	2–3	16.04	39.85	0.82
	100	0	2–3	18.83	45.08	0.65
	20	0	3–4	5.41	16.93	5.21
C2	20	2	2–3	1.56	12.43	5.89
	30	2	2–3	1.95	15.02	4.58
	50	2	2–3	2.54	19.22	2.04
	80	2	2–3	3.14	23.85	0.96
	100	2	2–3	3.46	26.42	0.74
	20	2	3–4	1.67	12.65	5.88

mean of local imbalances, decreases with decreasing measuring height. This finding, and the fact that observation heights are often lower than those used in Ka04, point out the need to investigate whether the imbalance mechanism stated by Ka04 is also of importance nearer to the surface.

Table 2 gives a summary of the imbalance statistics from our simulations with high spatial resolution; all imbalance statistics have been derived for an averaging period of 1 h. Keep in mind that Kanda et al. (2004) have shown that imbalance statistics depend clearly on the averaging period, so that all of the results presented will change at least quantitatively if the averaging period is altered. However, 1 h is a typical value for the averaging period used in field experiments. Moreover, note that in LES the representative heat flux consists of a resolved scale flux and a parameterised subgrid-scale (SGS) flux. Here, for all heights the SGS component is smaller than 6% and has a negative correlation with the imbalance, so that its impact on the imbalance statistics is almost neglegible.

According to Table 2, at a height of 100 m the imbalance statistics are of the same magnitude as those in Ka04. Moreover, our high-resolution simulations confirm, independently from the value of the geostrophic wind, Ka04's result that the imbalance and the spatial variability of temporal EC fluxes increase with the observation height. These findings are also reflected in Fig. 1, which shows the imbalance probability density function p, defined by

$$p(I) = \frac{N(I)}{N_t dI}, \tag{17a}$$

$$\int\limits_{-\infty}^{+\infty} p(I) \, dI = 1, \tag{17b}$$

where I is the local imbalance defined by Eq. 9, dI is the increment of I, N_t is the total number of grid points for an analysed horizontal cross-section and $N(I)$ is the number of grid points within the imbalance interval $[I - 0.5dI, I + 0.5 \, dI]$. The increase of the spatial variability of fluxes with increasing observation height corresponds to the

Fig. 1 Imbalance probability density functions at the different observation heights of run C1. Averaging period: 4–5 h
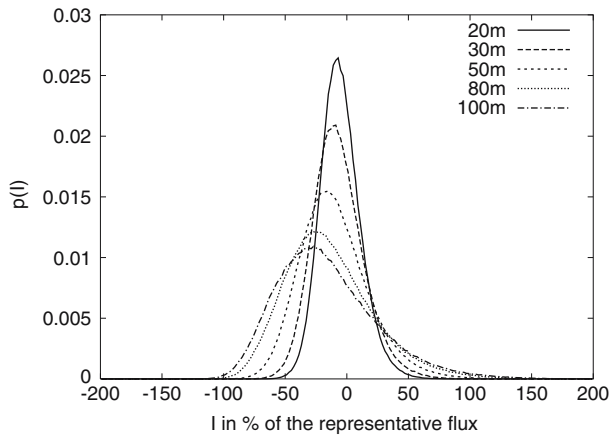
widening of p, while the decrease of the mean imbalance with decreasing observation level corresponds to a shift of the maximum of p towards 0.

The most important information contained in Table 2 and Fig. 1 is that a clear dependency of the imbalance statistics on height is found: the lower the observation level, the smaller becomes the absolute value of the imbalance. Even at our lowest observation height of 20 m a systematic underestimation of the representative flux is evident. However, it is one order of magnitude smaller than the imbalances that are usually reported for field experiments and also considerably smaller than the imbalances at a height of 100 m (the standard observation height in Ka04). Applying the explanation given by Ka04, the imbalance can be linked to the existence of TOS that can still be identified also at 20 m (Fig. 2). According to Schmidt and Schumann (1989) the TOS at different heights are correlated with each other. Here, the correlation coefficient for TOS between 20 and 100 m height is 0.82. However, the TOS at a height of 20 m are weaker than those at 100 m (Fig. 2). The smaller mean vertical velocities cause smaller local advection terms, and finally result in a smaller mean of the local advection term. Simultaneously, the representative heat flux decreases linearly with increasing height, as the simulated boundary layer is in a quasi-stationary state. According to Eq. 10 this leads to a decrease of mean imbalances with decreasing height. Moreover, there seems to be a loss of distinctiveness in the shape of TOS with decreasing height, i.e. the edges of convergence lines become more ambiguous. This is due to the increasing importance of smaller-scale turbulent eddies. The smaller the distance between the observation height and the surface, the smaller is the diameter of the largest turbulent eddies and the smaller is the integral time scale. This leads to an increasing statistical stability of the sampling of eddies: the smaller is the diameter of turbulent eddies, the higher is the number of eddies passing through a certain observation point during a fixed averaging period (Rannik and Vesala 1999). This mechanism also contributes to the smaller variability of mean vertical velocities at the lower observation height, which results in the smaller mean imbalances. Moreover, it also reduces the spatial variability of fluxes. Ka04 have shown that a low-frequency trend in the time series of the potential temperature and in the time series of the vertical velocity can cause large local imbalances, if these trends are correlated or anticorrelated respectively with each other. While the temperature trend at two different levels is expected to be similar, the time series of the vertical velocity shows more
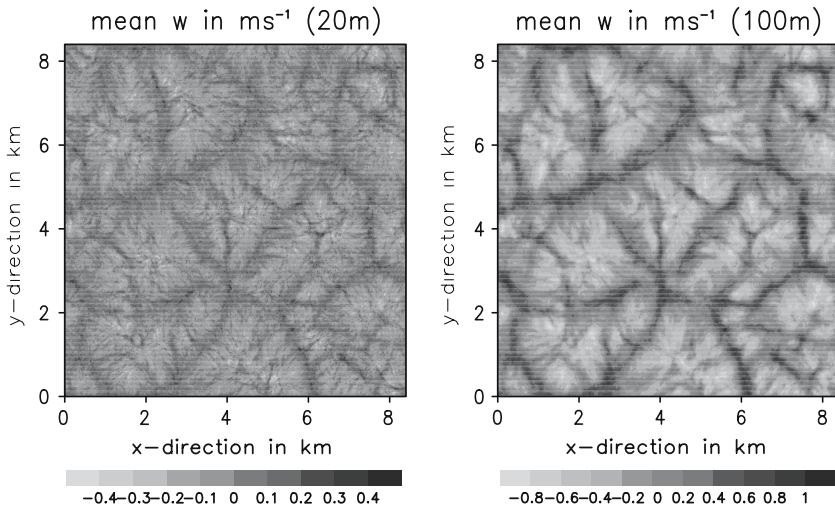
Fig. 2 Vertical velocity maps with 1-h averaging (period: 4–5 h) obtained in run C1 at heights of 20 m (left) and 100 m (right)

frequent changes between updraughts and downdraughts nearer to the ground, which enables more effective balancing between positive and negative contributions to the EC flux and thus smaller local imbalances. However, Table 2 reveals that even at a height of 20 m the variability of fluxes is of the same magnitude as determined at a height of 15.5 m by Katul et al. (1999) (17%). However, we have to be aware that Katul et al's (1999) measurements were made in the roughness sublayer above a pine forest, so that a direct comparison is not justified. Nevertheless, the LES results point to the importance of TOS contributions to the flux variability.

From our LES results we conclude that TOS cause flux underestimates also at heights found at small tower EC sites, but the mean imbalances are much smaller than those observed for such towers in the real atmosphere. The clear dependency of imbalance statistics on height leads us to expect that for near-surface energy balance stations, i.e. at heights of about 2 m, the mean imbalance caused by TOS will be completely negligible e.g. if compared with the systematic and random errors of a flux measurement related to the sensor. Therefore, Ka04's explanation for imbalances is insufficient to explain the lack of energy closure in most field experiments (except for tower measurements). Nevertheless, the wide spatial variability of fluxes at low observation levels underlines the difficulty of using the temporal EC method for an evaluation of representative fluxes even in an idealised, homogeneous domain.

4.2 Effect of a variation of the near-surface heat flux

We now investigate the impact of different parameters on imbalances and on the spatial variability of temporal EC fluxes, because such a sensitivity study may help to identify conditions for field experiments where TOS-generated imbalances are expected to be small.

Table 3 comprises the imbalance statistics obtained for a set of simulations with near-surface heat fluxes ranging from 0.05 to 0.4 K m s^{-1} both for $u_g = 0$ m s^{-1} and $u_g = 2$ m s^{-1} (simulation runs C3–C12).
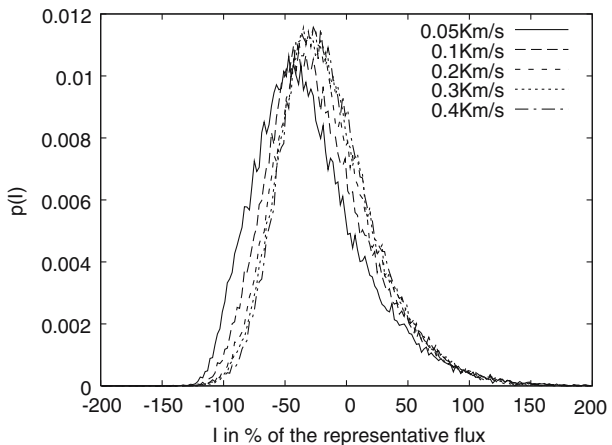
Table 3 Imbalance statistics for runs with varying values of the near-surface heat flux. $\partial[\Theta]/\partial tF_r$: ratio of the trend of the horizontal mean potential temperature and the representative heat flux; for the remaining abbreviations see captions of Tables 1 and 2.

Run	u_g (m s^{-1})	F_Θ (K m s^{-1})	F_r (K m s^{-1})	t_p(h)	$[I]$ (%)	σ_I (%)	SGS (%)	$\frac{\partial[\Theta]}{\partial tF_r}$ (s h^{-1} m^{-1})
C3	0	0.05	0.045	2–3	29.34	54.08	4.99	4.39
C4	0	0.10	0.091	2–3	21.06	47.98	5.05	3.70
C5	0	0.20	0.183	2–3	16.92	43.79	5.04	3.33
C6	0	0.30	0.277	2–3	15.10	42.04	5.02	3.05
C7	0	0.40	0.372	2–3	13.40	40.99	5.05	2.84
C8	2	0.05	0.045	2–3	3.69	23.70	5.22	4.33
C9	2	0.10	0.091	2–3	3.81	24.64	5.12	3.72
C10	2	0.20	0.184	2–3	4.59	27.59	5.15	3.31
C11	2	0.30	0.277	2–3	4.58	28.52	5.17	3.03
C12	2	0.40	0.372	2–3	5.22	27.84	5.22	2.83

According to Table 3 there is a quite clear decrease of the horizontal mean of imbalances with an increasing near-surface heat flux in the case of zero geostrophic wind. Moreover, the spatial variability of fluxes also decreases when the near-surface heat flux is increased. Figure 3 shows the imbalance probability functions for the different near-surface heat fluxes without a mean wind. It reflects the increase of the spatial variability of local flux estimates by showing a widening of the imbalance probability function for smaller near-surface heat fluxes. The decrease of the mean imbalance is reflected in a shift of the maximum of the imbalance probability density function towards less negative imbalances for larger near-surface heat fluxes. According to Ka04 the larger maximum positive and negative imbalances in the case of a lower near-surface heat flux might be due to the existence of larger low-frequency trends in the time series of the turbulent quantities. In the following, we try to derive an explanation for this hypothesis.

As the entrainment heat flux at the top of the boundary layer, $[\overline{F}](z_i)$, can be related to the near-surface heat flux, $[\overline{F}](0)$, the temporal change of the horizontally- and temporally-averaged temperature within the CBL can be written as

Fig. 3 Imbalance probability density functions for different near-surface heatfluxes and zero u_g

$$\frac{\partial \left[\overline{\Theta}\right]}{\partial t} = -\frac{\left[\overline{F}\right](z_i) - \left[\overline{F}\right](0)}{z_i} = \alpha \frac{\left[\overline{F}\right](0)}{z_i}. \tag{18}$$

For a detailed derivation of this equation see e.g. Stull (1988). As the local imbalance is expressed as a fraction of the representative flux, also the temperature trend is set in relation to the representative flux in order to assess its impact on local imbalances. Thus, we obtain some kind of relative temperature trend

$$\frac{\partial \left[\overline{\Theta}\right]}{\partial t}(z) \bigg/ \left[\overline{F}\right](z) = \alpha \frac{\left[\overline{F}\right](0)}{z_i \left[\overline{F}\right](z)}. \tag{19}$$

If we finally replace $\left[\overline{F}\right](z)$ by explicitly applying the appropriate linear function

$$\left[\overline{F}\right](z) = \left[\overline{F}\right](0) + \frac{\left[\overline{F}\right](z_i) - \left[\overline{F}\right](0)}{z_i} z = \left[\overline{F}\right](0) \left(1 - \alpha \frac{z}{z_i}\right), \tag{20}$$

Eq. 19 can also be expressed as

$$\frac{\partial \left[\overline{\Theta}\right]}{\partial t}(z) \bigg/ \left[\overline{F}\right](z) = \frac{\alpha}{z_i - \alpha z}. \tag{21}$$

Thus, if the analysis period and all initial conditions except the near-surface heat flux are identical in two different simulation runs, provided also that α is comparable, the relative temperature trend is smaller in the simulation with the higher near-surface heat flux, since the height of the boundary layer z_i is higher in that case. Therefore, the larger relative temperature trend in the case of the small near-surface heat flux causes the widening of the imbalance probability density function.

Another question is how the decrease of the mean imbalance with an increasing near-surface heat flux can be explained. Here, we suggest the following hypothesis starting with Ka04, who concluded from the low-frequency trends in the time series of w and Θ that the TOS are moving with time. Moreover, they also associated the decrease of mean imbalances in cases of longer averaging periods with movements of TOS. Due to the increased energy input with increased near-surface heat flux, we expect that the drifting velocity of the TOS increases with an increase of the near-surface heat flux. One hint for the validity of this assumption is the increase of horizontal velocity variances with increasing near-surface heat flux. Ka04 pointed out that the mean imbalance decreases with an increase in the geostrophic wind, as the advection of TOS with the mean wind weakens the mean vertical advection. Similar consequences are caused by larger drifting velocities.

If a geostrophic wind of $2 \, \mathrm{m \, s}^{-1}$ is prescribed, a completely different behaviour of imbalance statistics with a change of the near-surface heat flux is observed (Table 3): instead of a clear decrease with increasing near-surface heat flux as in the zero mean wind case, a slight increase of imbalances is apparently obtained. Of course, also for this series of simulations the largest relative temperature trend is observed in the temperature time series of the simulation with the smallest near-surface heat flux (Table 3). According to the paragraphs presented above, one could perhaps expect that also the imbalances would be largest in that case. However, as has been pointed out in many previous studies (e.g. Ka04; Mahrt 1998; Lee 1998; Wilson et al. 2002), the impact of the relative temperature trend on imbalances is considerably weakened

by an increase of the mean wind speed. Therefore, we checked the mean wind speed, averaged over the period of the flux evaluation, in the observation level of 100 m in our simulation series with $u_g = 2\,\mathrm{m\,s}^{-1}$. Indeed, we found slightly smaller mean wind speeds in the cases of larger near-surface heat fluxes. Obviously, this causes the slight increase of imbalances with increasing near-surface heat flux. This result underlines that the effect of the mean wind speed on imbalances is stronger than that of a change of the near-surface heat flux.

4.3 Effect of strong geostrophic winds

Ka04 investigated the impact of the magnitude of the mean ambient wind on the mean imbalance, for geostrophic winds up to $4\,\mathrm{m\,s}^{-1}$. With an increase of the geostrophic wind the temporally-averaged TOS became weaker due to the advection of cellular structures with the mean wind, causing a decreased imbalance.

Field measurements (LeMone 1973) have shown that in a moderately convective boundary layer horizontal roll vortices instead of cells can form that align with the mean wind. Several prior LES studies have been successful in the simulation of such vortices, e.g. Khanna and Brasseur (1998), Moeng and Sullivan (1994) and Sykes and Henn (1989). In these studies the existence of roll vortices has been observed for values of the stability parameter $-z_i/L$ between 1.5 and 10, where z_i is the boundary-layer height and L is the Obukhov length.

We looked at whether the change from cellular to roll-like convection has an influence on the imbalance by comparing the imbalance statistics at a height of 100 m for the simulation with $u_g = 2\,\mathrm{m\,s}^{-1}(-z_i/L = 155)$ and one with $u_g = 15\,\mathrm{m\,s}^{-1}(-z_i/L = 2.6)$. Indeed, in the latter case a roll-like structure was observed (Fig. 4) as in a similar simulation described in Khanna and Brasseur (1998). According to Fig. 4 the horizontal distance between two neighbouring updraught regions is about 2.5–3 km, which compares fairly well with Khanna and Brasseur's (1998) value of approximately $2z_i$.
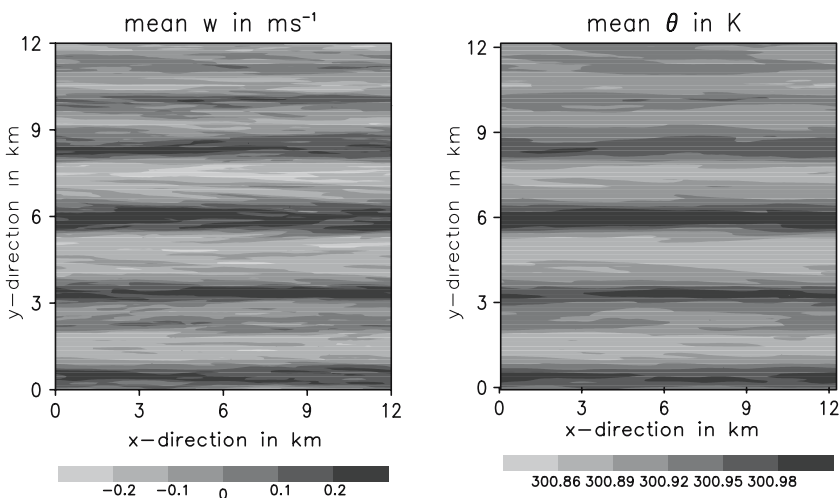

Fig. 4 Vertical velocity (left) and potential temperature map (right) with 1-h averaging (period:2–3 h) obtained for run C15 at a height of 100 m

Table 4 reveals that the change from cell-like to roll-like convection is accompanied by an increase of the mean imbalance. Thus, the finding of Ka04 that an increase in the geostrophic wind leads to a decrease in the imbalance is valid only if there is no fundamental change in the convection pattern. During roll-like convection plumes and thermals align in rows almost parallel to the mean wind. From this it follows that the advection of these plumes and thermals does not cause a significant weakening of the TOS, because most of the virtual observation points are situated during the whole averaging period either in an updraught/warm or in a downdraught/cool region. Even in the temporally-averaged fields of the vertical velocity w and the potential temperature Θ alternating streaks of updraughts/downdraughts and warm/cool regions are observed respectively, which are aligned in the direction of the mean wind, correlated with each other and extending across the whole model domain (Fig. 4). The difficulty of gaining accurate flux estimates from tower measurements when a roll-like convection pattern is observed has already been reported by Mahrt (1998), who found that the elongation of eddies in the downwind direction could lead to serious sampling problems and a considerable contribution of the mean flow to the total flux. Similar observations concerning increased imbalances related to roll-like turbulent structures were made by Inagaki et al. (2006) in their study on heat flux imbalances over horizontally inhomogeneous terrain. In that case a thermally-induced mesoscale, roll-like, circulation formed due to the inhomogeneous heating from the ground.

From our results we conclude that the concept of single tower measurements fails in the presence of roll convection. Instead horizontally distributed measurement networks are required.

4.4 Imbalance of fluxes in the SBL

Within the SBL the generation of turbulence is dominated by mechanical production. Naturally, the TOS described above do not occur in the SBL (and will not cause any imbalance). Nevertheless, we carried out a simulation for an SBL, based on Arctic observations, in order to determine whether imbalances occur under moderately stable stratification.

Table 5 reveals that at least under moderately stable stratification in the SBL the horizontal mean of local imbalances vanishes at all heights. It also shows that the SGS contribution to the total flux is rather high, compared with all previously described runs. We are aware that due to this rather large contribution the corresponding imbalance statistics at our lowest observation level (4 m) need very careful interpretation. However, there are several hints that a near-zero imbalance at a height of 4 m is indeed a characteristic of the horizontally homogeneous SBL. The first hint is that the imbalance is near zero also at a height of 50 m, where the SGS component, according to Table 5, is nearly negligible. The other hint is that from our analysis of imbalances

Table 4 Imbalance statistics for the runs with moderate and strong geostrophic winds. All abbreviations are explained in the captions of Tables 1 and 2

| Run	u_g (m s^{-1})	F_Θ (K m s^{-1})	t_p (h)	[I] (%)	σ_I (%)	SGS (%)
C4	2	0.05	2–3	3.69	23.70	5.22
C15	15	0.05	2–3	9.51	24.17	18.03

Table 5 Imbalance statistics for the simulation of the SBL. All abbreviations are explained in the captions of Tables 1 and 2

Run	z_a (m)	F_Θ (K m s^{-1})	t_p (h)	$[I]$ (%)	σ_I (%)	SGS (%)
S1	4	−0.0075	10–11	0.11	−5.13	58.24
	10	−0.0075	10–11	0.11	−6.67	20.90
	20	−0.0075	10–11	0.08	−6.99	10.40
	30	−0.0075	10–11	0.05	−6.12	8.27
	40	−0.0075	10–11	0.02	−6.28	7.60
	50	−0.0075	10–11	0.02	−5.23	7.16

in the CBL it is quite obvious that imbalances are observed whenever large-scale turbulent structures cause low-frequency trends in the time series of the vertical velocity that interact with the (diurnal) trend in the time series of the potential temperature. Since a grid spacing of 2 m should be sufficient to resolve possible large-scale structures in the SBL, simulations with a finer resolution would of course lead to a better resolution of the smaller-scale structures (and hence reduce the SGS fluxes) but should have no significant effect on the imbalance.

As can be gathered from Fig. 5 streak-like structures exist in the temporally-averaged fields of vertical velocity and potential temperature, but these structures are very weak, e.g. the difference between the highest and lowest mean vertical velocity is about 0.02 m s^{-1}, which is two orders of magnitude smaller than in the CBL. Moreover, the mean vertical velocity does not seem to be correlated with the mean potential temperature. This is underlined by a rather low correlation coefficient of −0.4, and so the horizontal mean of local advection terms becomes marginal.

Furthermore, Table 5 reveals that the standard deviation of temporal EC fluxes in the SBL is significantly smaller than that in the CBL. This can be explained by the fact that, in contrast to the CBL, a low-frequency trend in the time series of the vertical velocity cannot be observed (Fig. 6). Instead, a frequent change between updraughts
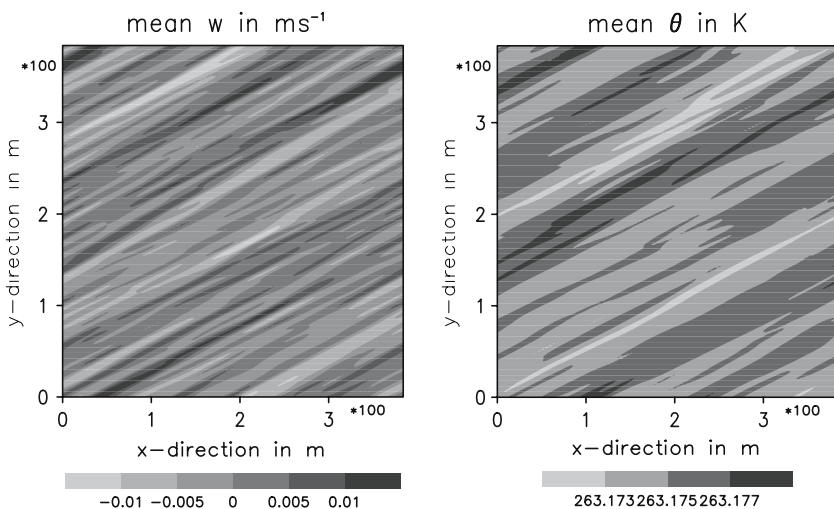
Fig. 5 Vertical velocity (left) and potential temperature map (right) with 1-h averaging (period:10–11 h) obtained in run S1 at a height of 50 m
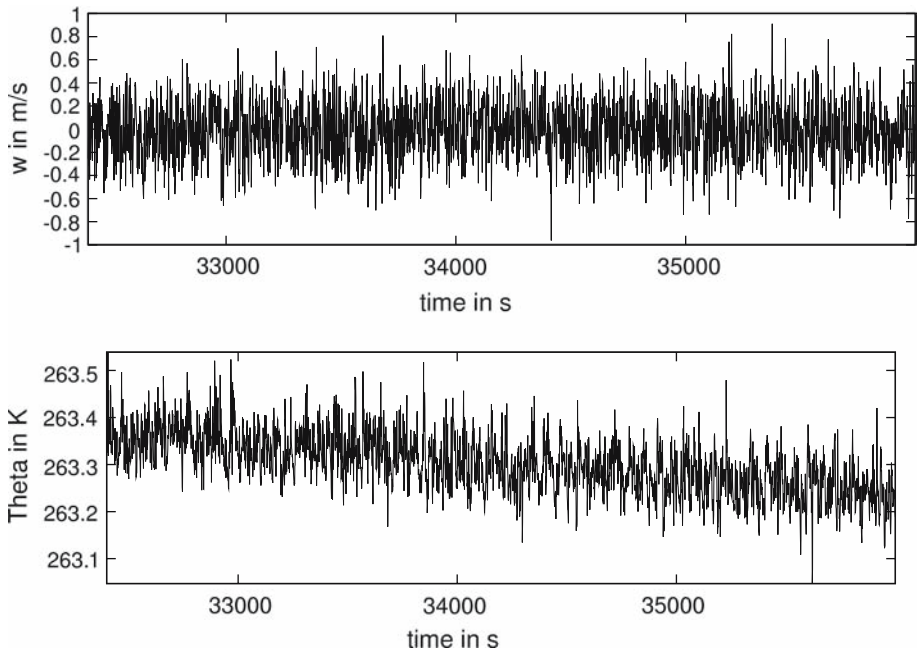
Fig. 6 Time series of vertical velocity (top) and potential temperature (bottom) recorded at the observation point with the largest local imbalance at a height of 50 m for the period 9–10 h of run S1

and downdraughts is detected and the rather low correlation coefficient reveals that these changes are poorly correlated with changes in the time series of the potential temperature.

In summary, we conclude that the imbalances obtained in real field experiments under stable stratification (Foken 2003) cannot be explained by the mechanism suggested by Ka04 for the CBL. Other possible causes for the lack of energy closure in the SBL are discussed in detail by Massman and Lee (2002).

5 Filtering methods and their impact on imbalance

The EC method is based on a minimum of prerequisites (e.g. Foken and Wichura 1996), but even these are never met completely in the real atmosphere (Rannik and Vesala 1999). For example, while the EC method basically requires a stationary flow, the diurnal cycle produces low-frequency changes in the time series of turbulent quantities. Often, attempts are made to remove these trends by high-pass filtering, in order to improve the accuracy of flux estimates. Great care is needed for the application of high-pass filtering since inappropriate filters might damage physically meaningful turbulent components (Caramori et al. 1994; Rannik and Vesala 1999). The difference between the horizontally-averaged temporal EC flux $\overline{[w'_t \Theta'_t]}$ and the temporally-averaged spatial EC flux $\overline{[w'_s \Theta'_s]}$ indicates how an appropriate filtering technique must be designed in order to correct the non-filtered EC fluxes in such a way that a systematic underestimation of the representative flux is prevented. No

filter should be used for the turbulent fluxes $\overline{\left[w_s'\Theta_s'\right]}$, which provide an ideal estimation of the representative flux. In contrast, for the turbulent fluxes $\overline{\left[w_t'\Theta_t'\right]}$, high-pass filtering should be used only for the transported quantity, but not for the vertical velocity (there is no diurnal trend of w), and the filter should be chosen to match as closely as possible the trend of the horizontal average of the transported quantity. If we use a high-pass filter only for the time series of temperature Θ, then the instantaneous temperature is decomposed into a low frequency trend component $\langle\Theta\rangle$ and a corresponding deviation Θ'_{filter}:

$$\Theta = \Theta'_{\text{filter}} + \langle\Theta\rangle. \tag{22}$$

The application of this decomposition in Eq. 2 leads to

$$\left[\overline{F}\right] = \overline{\left[w\,\langle\Theta\rangle\right]} + \overline{\left[w\Theta'_{\text{filter}}\right]} + \left[\,\overline{w\Theta_b}\,\right]. \tag{23}$$

If the filter function $\langle\Theta\rangle$ is chosen to be identical with $[\Theta]$, then Eq. 22 is equivalent to Eq. 5, and provided that the horizontal mean w vanishes, there will be no bias in EC flux estimates. Therefore, it is sufficient to carry out high-pass filtering only for the transported quantity Θ, and the filter function $\langle\Theta\rangle$ should be determined to match $[\Theta]$ as closely as possible.

For specific CBL simulations the effects of two high-pass filters on the horizontal mean of local imbalances and the spatial variability of fluxes were examined. At first the linear detrending (LDT) method was applied, which is widely used for the post-processing of real atmospheric EC data, and according to Rannik and Vesala (1999) preferable to other filter methods, although they have already pointed out some of its disadvantages. The high-pass filtering effect of the LDT method depends on the flux-averaging period, and for commonly used averaging periods the systematic errors of fluxes after filtering are often not negligible, since the LDT method does not only remove the trend but sometimes also removes important low frequency contributions, e.g. those caused by the movement of TOS with a time scale longer than the averaging period. Moreover, second-order or higher-order trends cannot be removed by the linear detrending method. Within the LDT method a linear function regressed from local time series of the transported quantity is employed at each observation point (filter A: $\langle\Theta\rangle = c_1t + c_2$, where $c_1(x, y)$, $c_2(x, y)$ are constants and t is time). Additionally, for test cases we also applied a corresponding high-pass filter to the time series of the vertical velocity (filter B: A and $\langle w\rangle = c_3t + c_4$). For the regression analysis the least-squares method was applied. The third filter uses $[\Theta]$ (filter C: $\langle\Theta\rangle = [\Theta]$). Filters A and B are applicable for any single point measurement, whereas filter C needs idealised multi-point measurements. Fig. 7 shows the imbalance probability functions obtained with filtering, and Table 6 summarises the corresponding imbalance statistics. Even filtering with linear functions reduces the spatial variation of local flux estimates. Moreover, there is no difference between the results that were obtained with filters A and B. Concerning the negative biases of the area-averaged imbalance, the application of filters A and C results in controversial conclusions (Table 6). The filter using the horizontally-averaged temperature trend eliminates the negative bias in the imbalance completely. In contrast, the local filter using linear regression even increases the mean imbalance by a factor of about two. Thus, it cannot be recommended to use the method of linear detrending in order to determine an estimate of

Fig. 7 Imbalance probability density functions obtained without filtering and with application of filter methods A, B and C, respectively for simulation C11. Averaging time: 1 h; period: 4–5 h; observation height: 100 m. No differences between the results for filters A and B can be detected
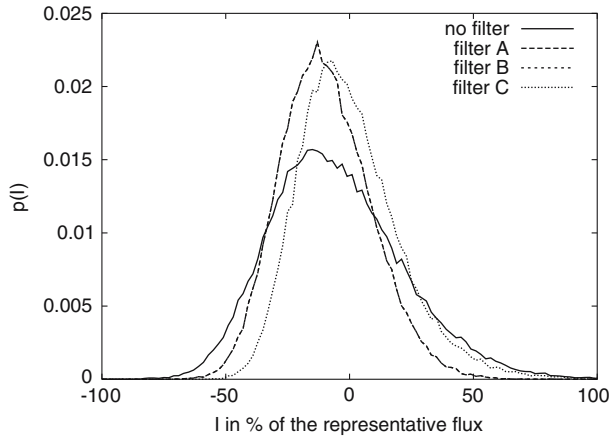

Table 6 Imbalance statistics obtained without and with application of a filter. All abbreviations are explained in the caption of Table 1

Run	filter method	t_p (h)	$[I]$ (%)	σ_I (%)	$I < -10$ (%)
C10	no filter	3–4	5.1	27.1	46.3
	filter A	3–4	9.7	20.7	51.7
	filter B	3–4	9.7	20.7	51.7
	filter C	3–4	0.0	20.8	34.2

the representative flux. In contrast, additional measurements of the temperature at as many observation points as possible are recommended in order to determine its area-averaged trend. The discussion above points out the limitation of single-tower measurements since either direct multi-point measurements or the suggested filter require horizontally distributed observation networks.

Figure 8 shows that, even in realistic cases where EC measurements are only carried out at a few observation points, the new filter method is potentially a powerful tool for reducing imbalances. Moreover, it reveals that a prerequisite for a successful application of the new filter is the availability of an accurate estimate of the horizontal mean potential temperature, which could be derived from e.g. an additional dense network of comparatively cheap low response temperature sensors. In more than two-thirds of the investigated cases, where the representative heat flux was evaluated as the mean of three local EC fluxes, a reduction in the imbalance was achieved when an accurate value of the horizontal mean temperature was used. In contrast, averaging of the EC fluxes at about 25 EC sites is necessary to achieve a comparable rate of improvement, when only an approximation of the mean temperature derived from the measurements at those 25 sites is used for filtering.

On the basis of these results we recommend the measurement of temperature with low response sensors at a large number of sites, in addition to the measurements at the EC sites, and to apply the new filter method in order to reduce imbalances.

🍎 Springer

Fig. 8 The diagram shows the percentage of 2000 randomly selected combinations of *n* virtual observation points from a total of 57,600 gridpoints that exhibit an improvement in the flux estimate after the application of the new filter method for run C11. *a*: the mean of the potential temperature at the *n* selected observation points was used as estimation of the actual mean potential temperature. *e*: the actual mean potential temperature was used. The line indicates the horizontal mean imbalance without filtering
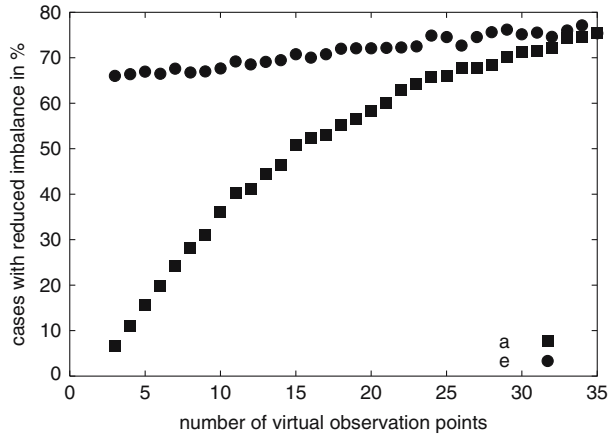
6 Summary and conclusions

Our simulations generally confirmed the findings of Ka04 that the energy imbalance, observed in many field experiments, can be caused by turbulent organised structures (TOS), which create low frequency trends in time series.

However, high resolution simulations showed that at low observation heights ($\leq 20\,\text{m}$) the imbalance is significantly smaller ($<5\%$) than for near-surface field experiments, where it sometimes exceeds 30%. Hence, although the TOS mechanism has a big effect on EC fluxes from (small) towers, it cannot account for the large imbalances observed at surface energy balance stations.

Nevertheless, we were able to confirm for the CBL that the temporal EC method is not an appropriate tool to derive accurate estimates of the representative flux, if it is based on measurements of turbulent quantities at only a few sites within the horizontal area under investigation. A considerable spatial variability of EC fluxes is observed even at low observation levels.

The effect of the geostrophic wind on EC fluxes depends on the convective regime. The mean imbalance decreases with increasing wind, so long as cellular convection prevails. For higher geostrophic winds, when the cellular convection switches to a roll-type convection, the imbalance increases again, because at many observation points there is no longer a balance between updraught and downdraught periods, and thus the contribution of the mean transport becomes more important again.

Due to the lack of TOS, our analysis of the simulation data of a moderately stable regime did not show any significant imbalance. Under this regime, the temporal EC method seems to be an appropriate tool for determining the representative flux, if a horizontal network of EC measurements is available. However, there is still a considerable variability of single EC fluxes, which raises the question as to whether single ground-based measurements provide the representative flux with a high accuracy even under these conditions.

springer

The evident imbalances in the CBL reveal that the EC method alone is not able to produce accurate estimates of the representative flux. Ka04 found out that the low-frequency trends in the measured time series are responsible for the wide spatial variability of flux estimates. Therefore, an elimination of such low-frequency trends by an appropriate filter seems to be a promising tool for the reduction of local imbalances. The results of our study show that the hitherto widely used filter method of linear detrending, on the one hand, reduces the spatial variability of fluxes, but on the other hand, it worsens the problem of a systematic underestimation of fluxes. Thus, the linear detrending method cannot be recommended as a standard tool for the postprocessing of EC measurements. Instead, a new filter method, using the horizontal mean of temperature, has been derived, which leads to a completely vanishing horizontal mean of local imbalances and reduces the spatial variability of local fluxes. However, a prerequisite for the successful application of this new filtering method is the availability of a highly accurate estimate of the horizontally-averaged temperature. Therefore, an additional measurement network will be necessary that provides such an estimate, and to operate alongside the EC measurement sites within the area under investigation.

Overall, our study points out the limitation of single site measurements and the necessity of horizontally-distributed observation networks. If a horizontally dense network of EC measurement sites in real field experiments is too expensive, we recommend that measurements be made with the objective of determining representative fluxes by the temporal EC method as near to the ground as possible, and to avoid the application of the linear detrending method. Instead, we suggest filtering the measured time series with the horizontal mean value of the transported quantity, provided that it is available.

The discrepancy between the magnitude of imbalances observed in field experiments and in our near-surface simulation data indicates the need to further investigate possible causes of the large real field imbalances. For example, Inagaki et al. (2006) recently showed that a heterogeneous surface may have a significant effect on the imbalance.

References

Beare RJ, Cortes MAJ, Cuxart J, Esau I, Golaz C, Holtslag AAM, Khairoutdinov M, Kosovic B, Lewellen D, Lund T, Lundquist J, McCabe A, Macvean MK, Moene A, Noh Y, Poulos G, Raasch S, Sullivan PP (2006) An intercomparison of large-eddy simulations of the stable boundary-layer. Boundary-Layer Meteorol 118:247–272

Bernhardt K, Piazena H (1988) Zum Einfluss der turbulenzbedingten Dichteschwankungen auf die Bestimmung turbulenter Austauschstrme in der Bodenschicht. Z Meteorol 38:234–245

Beyrich F, Richter SH, Weisensee U, Kohsiek W, Lohse H, de Bruin HAR, Foken T, Göckede, M, Berger F, Vogt R, Batchvarova E (2002) Experimental determination of turbulent fluxes over the heterogeneous LITFASS area: selected results from the LITFASS-98 experiment. Theor Appl Climatol 73:19–34

Bosveld FC, Beljaars ACM (2001) The impact of sampling rate on eddy-covariance flux estimates. Agric For Meteorol 109:39–45

Bosveld FC, Bouten W (2001) Comparing transpiration models with eddy-correlation observations for a douglas-fir forest. Agric For Meteorol 108:247–264

Caramori P, Schuepp P, Desjardins R, Macpherson I (1994) Structural analysis of airborne flux estimates over a region. J Climate 7:627–640

Deardorff JW (1980) Stratocumulus-topped mixed layers derived from a three-dimensional model. Boundary-Layer Meteorol 18:495–527

Foken T (2003) Angewandte meteorologie. Springer, Berlin, Germany, 290 pp

Foken T, Wichura B (1996) Tools for quality assessment of surface-based flux measurements. Agric For Meteorol 78:83–105

Inagaki A, Letzel MO, Raasch S, Kanda M (2006) The impact of the surface heterogeneity on the energy imbalance problem using LES. J Meteorol Soc Japan 84:187–198

Isaac PR, McAneney J, Leuning R, Hacker M (2004) Comparison of aircraft and ground-based flux measurements during OASIS95. Boundary-Layer Meteorol 110:39–67

Kanda M, Inagaki A, Letzel MO, Raasch S (2004) LES study of the energy imbalance problem with eddy covariance fluxes. Boundary-Layer Meteorol 110:381–404

Katul G, Hsieh C, Bowling D, Clark K, Shurpali N, Turnipseed A, Albertson J, Tu K, Hollinger D, Evans B, Offerle B, Anderson D, Ellsworth D, Vogel C, Oren R (1999) Spatial variability of turbulent fluxes in the roughness sublayer of an even-aged pine forest. Boundary-Layer Meteorol 93:1–28

Khanna S, Brasseur JG (1998) Three-dimensional buoyancy- and shear-induced local structure of the atmospheric boundary layer. J Atmos Sci 55:710–743

Lee X (1998) On micrometeorological observations of surface-air exchange over tall vegetation. Agric For Meteorol 91:39–49

LeMone MA (1973) The structure and dynamics of horizontal roll vortices in the planetary boundary layer. J Atmos Sci 30:1077–1091

Letzel MO, Raasch S (2003) Large-eddy simulation of thermally induced oscillations in the convective boundary layer. J Atmos Sci 60:2328–2341

Leuning R, Legg BJ (1982) Comments on "The influence of water vapor fluctuations on turbulent fluxes" by Brook. Boundary-Layer Meteorol 23:255–258

Mahrt L (1998) Flux sampling errors for aircraft and towers. J Atmos Ocean Tech 15:416–429

Massman WJ, Lee X (2002) Eddy covariance flux corrections and uncertainties in long-term studies of carbon and energy exchanges. Agric For Meteorol 113:121–144

Moeng CH, Sullivan PP (1994) A comparison of shear- and buoyancy-driven planetary boundary layer flows. J Atmos Sci 51:939–1022

Oncley SP, Foken T, Vogt R, Bernhofer C, Kohsiek W, Liu H, Pitacco A, Grantz D, Ribeiro L, Weidinger T (2002) The energy balance experiment EBEX-2000. In: Proceedings of the 15th symposium on boundary layer and turbulence, Wageningen, The Netherlands, American Meteorological Society, pp 1–4

Panin GN, Tetzlaff G, Raabe A (1998) Inhomogeneity of the land surface and problems in the parameterization of surface fluxes in natural conditions. Theor Appl Climatol 60:163–178

Raasch S, Etling D (1998) Modeling deep oceanic convection: Large-eddy simulation in comparison with laboratory experiments. J Phys Oceanog 28:1786–1802

Raasch S, Harbusch G (2001) An analysis of secondary circulations and their effects caused by small-scale surface inhomogeneities using large-eddy simulation. Boundary-Layer Meteorol 101:31–59

Raasch S, Schröter M (2001) PALM – a large eddy simulation model performing on massively parallel computers. Meteorol Z 10:363–372

Raasch S (cited 2006) PALM group. [Available online at http://www.muk.uni-hannover.de/~raasch/PALM_group/]

Rannik, Ü, Vesala T (1999) Autoregressive filtering versus linear detrending in estimation of fluxes by the eddy-covariance method. Boundary-Layer Meteorol 91:259–280

Schmidt H, Schumann U (1989) Coherent structure of the convective boundary layer derived from large-eddy simulation. J Fluid Mech 200:511–562

Schröter M, Bange J, Raasch S (2000) Simulated airborne flux measurements in a LES generated convective boundary layer. Boundary-Layer Meteorol 95:437–456

Stull RB (1988) An introduction to boundary layer meteorology. Kluwer Academic Publishers, Dordrecht, 666 pp

Sykes RI, Henn DS (1989) Large-eddy simulation of turbulent sheared convection. J Atmos Sci 46:1106–1118

Twine TE, Kustas WP, Norman JM, Cook DR, Houser PR, Meyers TP, Prueger JH, Starks PJ, Wesely ML (2000) Correcting eddy-covariance flux underestimates over a grassland. Agr For Meteorol 103:279–300

Webb EK, Pearman GI, Leuning R (1980) Correction of flux measurements for density effects due to heat and water vapor transfer. Quart J Roy Meteorol Soc 106:85–100

Wilson K, Goldstein A, Falge E, Aubinet M, Baldocchi D, Berbigier, P, Bernhofer C, Ceulemans R, Dolman H, Field C, Grelle A, Ibrom A, Law BE, Kowalski A, Meyers T, Moncrieff J, Monson R, Oechel W, Tenhunen J, Valentini R, Verma S (2002) Energy balance closure at FLUXNET sites. Agric For Meteorol 113:223–243